Surface Moistening Trends in the Northern North American Great Plains Increase the Likelihood of Convective Initiation

TOBIAS GERKEN, GABRIEL T. BROMLEY, AND PAUL C. STOY

Department of Land Resources and Environmental Sciences, Montana State University, Bozeman, Montana

(Manuscript received 20 June 2017, in final form 17 November 2017)

ABSTRACT

Land management impacts atmospheric boundary layer processes, and recent trends reducing the practice of summer fallow have led to increases in precipitation and decreases in temperature in the Canadian Prairie provinces during summer. It is unclear if such trends also impact the hydrometeorology of the adjacent U.S. northern Great Plains, parts of which have seen similar changes in land management. Here, MERRA-2 reanalysis data, eddy covariance observations, and a mixed-layer (ML) atmospheric modeling framework are combined to demonstrate that the likelihood of convectively preconditioned conditions has increased by approximately 10% since the mid-1980s and is now more sensitive to further decreases in the Bowen ratio (Bo) and maximum daily net radiation $R_{n,\max}$ in northeastern Montana. Convective season Bo in the study area has decreased from approximately 2 to 1 from the 1980s until the present, largely due to simultaneous increases in latent heat flux and decreases in sensible heat flux, consistent with observed decreases of summer fallow and increases in cropping. Daily net radiation R_n has not changed despite a significant decrease in May and June humidity lapse rates from the 1980s to present. Future research should determine the area of the U.S. Great Plains that has seen changes in the dynamics of the atmospheric boundary layer height and lifted condensation level and their crossings as a necessary condition for convective precipitation to occur and ascertain if ongoing changes in land management will lead to future changes in convective outcomes.

1. Introduction

The land surface and atmosphere are linked through the exchange of water and energy, which modulates boundary layer development and precipitation that feed back to surface–atmosphere exchanges (e.g., Koster et al. 2004; Seneviratne et al. 2006). One example of land–atmosphere feedbacks with implications for land management, water resources, and regional climate is found in the North American northern Great Plains. Since the 1970s, shifts in cropping systems that include the reduction of summer fallow (Lubowski et al. 2006; Long et al. 2014; Vick et al. 2016) have coincided with a summertime cooling trend (Betts et al. 2013, 2014; Mahmood et al. 2014) of up to 2°C, a 7% increase in relative humidity (RH), and a 10 mm decade^{-1} increase in precipitation over parts of the Canadian Prairie provinces (Gameda et al. 2007) and moistening that extends to northeastern Montana and the Dakotas (Fig. 1).

Such behavior is consistent with evidence for agriculture's influence on weather and climate (reviewed in Raddatz 2007). Vegetated surfaces increase evapotranspiration [related via the latent heat of vaporization to latent heat flux (LE)] at the expense of sensible heat flux H. These changes in surface energy partitioning toward lower Bowen ratios (Bo = H/LE) result in shallower and moister atmospheric boundary layers (ABLs) compared to bare soils (e.g., Gameda et al. 2007; Vick et al. 2016) or in some cases natural vegetation (e.g., McPherson et al. 2004; Mahmood et al. 2014). Given that land management and land cover change have considerable effects on surface temperatures (Luyssaert et al. 2014; Mueller et al. 2015; Bright et al. 2017) and impact the water cycle through evapotranspiration and increases in atmospheric moisture, research is merited to further study local and regional effects of land–atmosphere interactions. In this context, Betts et al. (2013) noted that increased evapotranspiration in the Canadian Prairie provinces was responsible for a 0.34 mm day^{-1} increase in growing season precipitation. It remains unclear if changes in agricultural management that are similar to those in the Canadian Prairies

Corresponding author: Tobias Gerken, tobias.gerken@montana.edu

DOI: 10.1175/JHM-D-17-0117.1

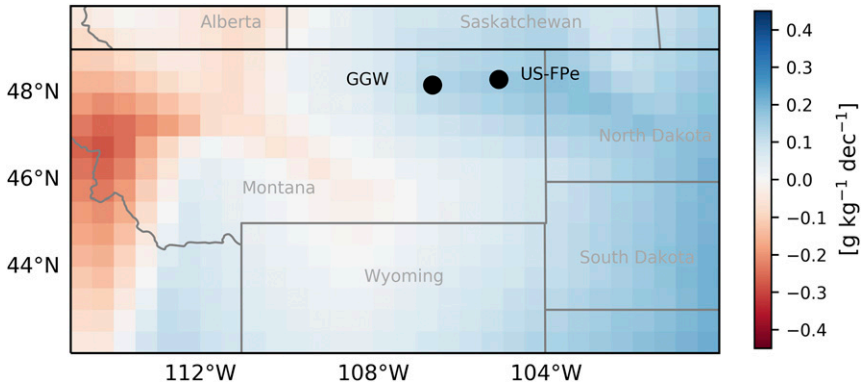

FIG. 1. The locations of the US-FPe eddy covariance research site and GGW atmospheric sounding site in Montana, with regional trends in specific humidity from 1970 until 2010 from the Climate Research Unit (CRU TS 3.10) database (Harris et al. 2014). Specific humidity was calculated using 2-m temperature, vapor pressure, and a 1000-hPa atmospheric reference pressure.

have impacted precipitation processes in adjacent regions of the United States (Vick et al. 2016) and, if so, what mechanisms underlie these changes.

Generally speaking, coupling in the land–atmosphere system is well documented: the coevolution between temperature and moisture in the mixed layer as well as surface flux partitioning presents several direct feedbacks. Heating or drying of the ABL increases evaporative demand by intensifying the vapor pressure deficit (VPD), which in turn increases LE under well-watered conditions. The subsequent moistening of the ABL presents a negative feedback to evapotranspiration (van Heerwaarden et al. 2009, 2010). Similarly, vegetation responds to VPD through stomatal regulation of transpiration when VPD exceeds a threshold of approximately 10 hPa (Körner 1995; Oren et al. 1999; Lasslop et al. 2010). The partitioning of net radiation R_n into H and LE is often expressed as evaporative fraction (EF) [$\mathrm{EF} = \mathrm{LE}/R_n = 1/(1 + \mathrm{Bo})$] (e.g., Kustas et al. 1993; Porporato 2009; Gentine et al. 2013a). EF (or Bo) tends to be conserved during the daytime (Crago and Brutsaert 1996; Gentine et al. 2007, 2011) and has direct impact on mixed layer (ML) heat and moisture contents as well as ML growth, which is driven by the buoyancy flux ($c_p\rho\overline{w'\theta_v'} \approx H$, with heat capacity of air c_p, air density ρ, and the covariance of vertical velocity and virtual temperature $\overline{w'\theta_v'}$). Shallow cumulus, formed when ascending air parcels reach the lifting condensation level (LCL), is a necessary prerequisite for generating moist convection, but not sufficient to directly diagnose precipitation (e.g., Juang et al. 2007a), as precipitation development further depends on the thermodynamic state of the atmosphere. Moist boundary layers are associated with higher moist static energies and are thus thermodynamically more prone to develop precipitating convection (e.g., Raddatz 1993; Segal et al. 1995; Yamada 2008; Brimelow et al. 2011). Consequently, surface energy partitioning directly impacts cloud formation, since greater H (and LE to a lesser degree) increases ML heights h, whereas greater LE decreases LCLs (Ek and Holtslag 2004), such that it is nontrivial to assess whether locally triggered convective precipitation is preferred over wet or dry surfaces. However, this is a crucially important question for assessing feedbacks in the energy and water cycles associated with drought (e.g., Findell and Eltahir 2003a, b; Ferguson and Wood 2011; Roundy et al. 2013; Gentine et al. 2013a; Ford et al. 2015; Guillod et al. 2015; Song et al. 2016). In addition to land surface and boundary layer processes, atmospheric stability and moisture contents also impact whether low-level clouds can grow to moist convection. Instances when convection development is independent of surface conditions are referred to as periods of atmospheric control (Findell and Eltahir 2003a,b). It is important to ascertain if convective precipitation is dependent on atmospheric control or both land surface and atmospheric triggers to understand the role of land surface change on convective precipitation.

Mixed layer (or slab type) models can provide valuable insight into these processes. They are computationally inexpensive and thus convenient for assessing land–atmosphere feedbacks and for quantifying the relationship between ecohydrological (e.g., surface flux partitioning) and atmospheric controls (e.g., atmospheric stability and moisture) on precipitation. ML models also have limitations. They are typically local in nature, such that regional circulation and large-scale effects are unaccounted for. Moreover, boundary layer structures and turbulent exchange across the capping inversion are prescribed, and accurate modeling of

cloud-topped boundary layers proves challenging due to the latent heat release from condensation, convective mass flux, and radiative effects, all of which impact boundary layer dynamics and growth (e.g., Stull 1988). Despite these limitations, simplified ML models have proven to be a valuable tool to investigate interactions between convection and soil moisture (e.g., Ek and Holtslag 2004; Juang et al. 2007a,b; Siqueira et al. 2009; Konings et al. 2010, 2011), convection and the groundwater table (Bonetti et al. 2015), the regulation of convective cloud formation above forests (Manoli et al. 2016), and impacts of land management on h (Vick et al. 2016). However, ML models have also been applied to diagnose the surface exchange of heat from boundary layer characteristics (Santanello et al. 2005; Gentine et al. 2013b) and extended to include thermodynamic quantities such as convective available potential energy (CAPE) as additional diagnostics (Yin et al. 2015). Such enhancements further refine slab-type models with the caveat that tendencies in the atmospheric profile that occur due to advection or diabatic warming, both of which impact thermodynamics, are not considered. Similarly, Findell and Eltahir (2003a,b) developed a framework to assess the thermodynamic state and the potential for convective development from atmospheric profiles of temperature and moisture (CTP–HI_{low}), which relates a convective triggering potential (CTP), related to the CAPE, to a low-level humidity index (HI_{low}) and demonstrated its applicability to wet and dry coupling behavior, namely, whether precipitation development is more likely over wet or dry soils.

The present work combines a mixed layer modeling approach with the CTP–HI_{low} framework to understand and quantify how changes in surface energy partitioning and atmospheric moisture have impacted the likelihood of convective initiation in a rapidly changing agricultural region in northeastern Montana (Long et al. 2014). The combined framework is applied to 1) investigate atmospheric and surface controls on the development of convective clouds and potential subsequent precipitation events, 2) identify the range of environmental parameters such as humidity and stability that lead to different convective outcomes, and 3) investigate the system's sensitivity to ongoing trends in surface energy–flux partitioning and atmospheric moisture supply.

2. Methodology

a. Data

Surface observations of H, LE, R_n, ground heat flux G, RH, air temperature T_{Air}, and surface pressure P_{Sfc} used in this work to describe current environmental conditions and to provide forcing for the slab model are from the AmeriFlux Fort Peck eddy covariance research site (station code US-FPe; Meyers 2000) located in northeastern Montana (48.31°N, 105.10°W, 634 m above mean sea level). Data are available from 2000 to 2008. The land cover at the site is a prairie grassland classified as cold semiarid steppe (BSk) in the Köppen–Geiger climate classification. Mean annual temperature and precipitation are 5.5°C and 335 mm.

Atmospheric sounding data were obtained for the period from 1975 to 2015 for the Glasgow International Airport in Montana (station code GGW), located approximately 110 km west of the Fort Peck site (48.21°N, 106.61°W). The airport is located to the northeast of the town of Glasgow and is surrounded by fields and grassland. Mixed layer evolution for the convective season, approximated here as the period between May and September, is based on the 1200 UTC profiles of T and moisture q, which correspond to approximately 0500 local time (LT). As ML development is driven by solar irradiance, all times used in this work are LT rather than UTC. Atmospheric lapse rates of potential temperature and humidity (γ_θ, γ_q) used in the model are calculated using a linear regression between 500 and 5000 m above ground level (AGL) similar to Manoli et al. (2016).

Modern-Era Retrospective Analysis for Research and Applications, version 2 (MERRA-2; Rienecker et al. 2011; Reichle et al. 2017; Gelaro et al. 2017), data are used to asses climatic surface trends in the region. Specifically, MERRA-2 land surface diagnostics comprising LE, H, and R_n, and provided at a spatial resolution of $0.5° \times 0.625°$, are studied to gain a long-term estimate of surface energy balance trends. Values are interpolated from the native MERRA-2 grid to the coordinates of the Fort Peck site using bilinear interpolation.

b. Model description

The model used to simulate mixed layer height development is described in detail elsewhere (Porporato 2009; Manoli et al. 2016). Briefly, assuming a constant Bo and parabolic behavior of the available energy for mixed layer growth between sunrise and sunset, Porporato (2009) derived an analytical solution for the diurnal evolution of the mixed layer height:

$$h = \left[\frac{2}{3}\frac{(1+2b)\,R_{n,\max}\,\mathrm{Bo}(3t_0 - t)\,t^2}{\rho\, c_p\, \gamma_0(1+\mathrm{Bo})\,t_0^2}\right]^{1/2}, \qquad (1)$$

where b is the ratio of sensible heat flux between h and the surface, often assumed to be 0.2 (e.g., Tennekes 1973; Driedonks 1982), $R_{n,\max}$ is the diurnal maximum of R_n, $\rho = 1.29\,\mathrm{kg\,m^{-3}}$ is the density of air, and $c_p = 1004.8\,\mathrm{J\,kg^{-1}\,K^{-1}}$ is its heat capacity. The temporal evolution is modeled for the interval $0 < t < 2t_0$, with

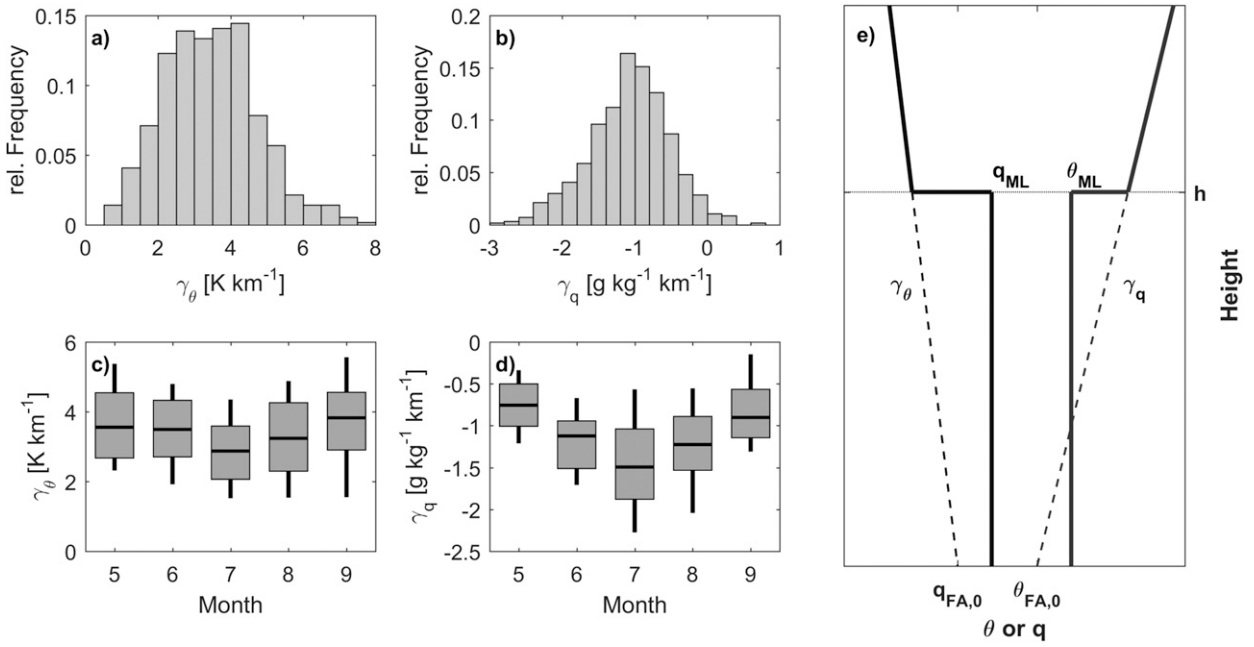

FIG. 2. Potential temperature and water vapor mixing ratio lapse rates [γ_θ (K km^{-1}) and γ_q (g kg^{-1} km^{-1}), respectively] observed at GGW for the convective season defined as May–September and days with observed eddy covariance flux data at US-FPe (2000–08): relative frequency for (a) γ_θ and (b) γ_q and box plots of the monthly distribution indicating median, interquartile range, and 10th and 90th percentile for (c) γ_θ and (d) γ_q. (e) A schematic drawing illustrating the relationship among θ_{ML}, γ_θ, and $\theta_{FA,0}$ as well as q_{ML}, γ_q, and $q_{FA,0}$.

0 and $2t_0$ as times of sunrise and sunset. Daytime is defined as the time when solar irradiance exceeds 25 W m^{-2}. In addition to the energy supplied by R_n, the growth of the mixed layer is controlled by the state of the atmosphere, which is represented by constant lapse rates of potential temperature γ_θ and water vapor mixing ratio γ_q. The evolution of mixed layer potential temperature θ_{ML} and moisture q_{ML} is given by

$$\theta_{ML} = \gamma_\theta \frac{1+b}{1+2b} \times h + \theta_{FA,0} \quad \text{and} \tag{2}$$

$$q_{ML} = \gamma_q' \times h + q_{FA,0}, \tag{3}$$

where $\theta_{FA,0}$ and $q_{FA,0}$ are the temperature and moisture at the intersection between the top of the ML and free atmosphere, respectively, which is extrapolated to the surface level, and γ_q' is the effective moisture lapse rate:

$$\gamma_q' = \frac{1}{2}\left[\gamma_\theta \frac{c_p}{\lambda(1+2b)\,\mathrm{Bo}} + \gamma_q\right], \tag{4}$$

with $\lambda = 2.45 \times 10^6$ J kg^{-1} as the latent heat of vaporization. The relationships between θ_{ML}, γ_θ, and $\theta_{FA,0}$ and their counterparts for q are illustrated in Fig. 2e.

The above equations constitute a closed system for modeling h, θ_{ML}, and q_{ML} that allows us to explore the atmospheric state (through γ_θ, γ_q, $\theta_{FA,0}$, and $q_{FA,0}$), surface energy partitioning related to surface moisture and surface conductance (related to Bo), and energy input into the system ($R_{n,\max}$) on h dynamics. It relies on a number of assumptions (Manoli et al. 2016): ML evolution is governed by local processes and large-scale convergence/divergence or advection of temperature and moisture are negligible, the ML is well mixed, and for each day Bo remains constant during the diurnal cycle. Also by definition, ML models are local in the sense that they assume flat topography and homogeneous surface conditions at scales sufficiently larger than h. Additionally, because of the chosen analytical framework, h is assumed to be zero before sunrise, similar to previous studies (Porporato 2009; Gentine et al. 2013a; Manoli et al. 2016). While this introduces an additional uncertainty to modeled h, the model's analytical nature reduces free parameters and allows for exploration of the system's sensitivities (see section 5).

The onset of shallow cumulus in mixed layer models is often assumed to occur when h exceeds the LCL (hereafter hxLCL). For the purpose of this study, it is also assumed that boundary layer clouds have the potential to develop when h exceeds the height of the LCL following the procedure outlined in Juang et al. (2007a). The LCL is given as (e.g., Stull 1988):

$$\mathrm{LCL} = \frac{\mathscr{R}_{\mathrm{air}}\theta}{g} \ln\left(\frac{P_{\mathrm{Sfc}}}{P_{\mathrm{LCL}}}\right), \tag{5}$$

with $\mathscr{R}_{air} = 287.06\,\mathrm{J\,kg^{-1}\,K^{-1}}$ as the gas constant for ambient air, g as gravitational acceleration, and P_{Sfc} and P_{LCL} as the pressures at the surface and LCL, where

$$P_{LCL} = P_{Sfc}\left(\frac{\theta_{LCL}}{\theta_{ML}}\right)^{7/2} \tag{6}$$

can be calculated using the potential temperature at the LCL, which can be estimated as (e.g., Stull 1988)

$$\theta_{LCL} = \frac{2840}{3.5\ln(\theta_{ML}) - \ln\left(\frac{q_{ML}P_{Sfc}}{0.622 + q_{ML}}\right) - 7.108} + 55. \tag{7}$$

Several previous studies have used the occurrence of boundary layer clouds as a necessary but not sufficient condition for the development of locally generated convective precipitation (e.g., Stull 1988; Juang et al. 2007a,b; Manoli et al. 2016), as air parcels overshooting the top of the cloud-topped ML may reach the level of free convection and become positively buoyant. Based on this framework, there are four possible states relating h and the onset of precipitation: 1) h reaches the LCL and a convective precipitation event is triggered, 2) h reaches the LCL, but boundary layer clouds do not sufficiently grow to trigger convective precipitation (or this precipitation is not realized at the measurement location), 3) there is no crossing of h and LCL and no precipitation occurs, or 4) h remains below the LCL but nonlocally triggered precipitation occurs (e.g., via a frontal system). Note that the ML model is only used in this work to diagnose the occurrence and timing of events where a crossing between h and the LCL occurs and not whether convective triggering occurs, which requires additional diagnostics. Similarly, the growth of h after exceeding the LCL should not be modeled using the analytical approach, as the convective mass flux associated with clouds (e.g., Stull 1988) and convection as well as the reduction of R_n is not included in the model.

c. Model setup

For each day, Bo is determined as the mean value between 1000 and 1500 LT, similar to Rigby et al. (2015), who suggested the use of the diurnal mean rather than daily maximum Bo to avoid overestimation of h. The maximum daytime net radiation $R_{n,max}$ is determined by fitting a parabolic profile to the daytime net radiation R_n, which is defined as $R_n \geq 25\,\mathrm{W\,m^{-2}}$ and is also used to determine $2t_0$. The model was run for each day during the convective season, except for days with precipitation occurring before 0900 LT and days during which $R_{n,max} < 25\,\mathrm{W\,m^{-2}}$. Similar to Manoli et al. (2016), and to exclude days in which h development is strongly influenced by shear, days during which the observed maximum friction velocity $u*$ exceeded the 90th percentile were also excluded. Also, such conditions indicate the likely influence of mesoscale convective systems through cold pool shear and squall lines, which cannot be modeled with the chosen approach. Gaps in turbulent flux measurements that lasted a single 30-min interval were gap filled using linear interpolation. Days that contained larger gaps in the observed H or LE, or when the daily integrated energy balance closure $[(H + \mathrm{LE} + G)/R_n$, with ground heat flux $G]$ was below 0.5 or exceeded 1.25, were excluded from the analysis.

The chosen approach to model h constitutes a simple but tractable model, which excludes the radiative and thermodynamic effects of clouds (see, e.g., van Stratum et al. 2014), detailed atmospheric profiles, and dynamic processes such as advection and subsidence. However, the inclusion of these would greatly increase the degrees of freedom in the analysis, which are not constrained by observations.

d. Coupling metrics

The CTP–$\mathrm{HI_{low}}$ framework (Findell and Eltahir 2003a,b), recently discussed by Roundy et al. (2014) and Ferguson and Wood (2011), is also used to characterize atmospheric controls over convection. The CTP is defined as the integrated area between a temperature sounding and a moist adiabat originating at 100 hPa AGL, which is followed up to 300 hPa AGL. As such, higher CTP indicates a thermodynamic state that is more permissive to convection. The lower troposphere humidity index ($\mathrm{HI_{low}}$, based on Lytinska et al. 1976), is defined from the dewpoint depressions at 50 and 150 hPa AGL:

$$\mathrm{HI_{low}} = \left(T_{50} - T_{d,50}\right) + \left(T_{150} - T_{d,150}\right), \tag{8}$$

where T and T_d are the temperature and dewpoint temperature at the pressure level indicated by the subscript, and $\mathrm{HI_{low}}$ is thus a measure of atmospheric dryness that can suppress convection. Coupling between the surface and atmosphere is classified similarly to the naming convention of Roundy et al. (2013) and based on the difference in modeled convective outcomes for different surface states represented by Bo. If decreasing the Bo leads to a crossing between h and the LCL, the surface is referred to as *wet coupled*, whereas for a *dry coupled* surface the reverse is true. If the convective outcome (either dry or wet) is independent of Bo, we consider the day to be under *atmospheric control*. For the purpose of this study, we determine the relationship between wet and dry coupling and the CTP–$\mathrm{HI_{low}}$

framework by dividing the GGW radiosonde profiles into classes of CTP and HI_{low}. The class width is $40\,J\,kg^{-1}$ for CTP and 2°C for HI_{low}. For each class, the slab model is executed for all pertaining radiosonde profiles using Bo ranging from 0.25 to 4. Coupling behavior is assigned if at least 75% of profiles for a given bin show the same coupling behavior; otherwise, the bin is considered to pertain to the transition between coupling states. Transition states are further subdivided according to the dominant coupling state. For example, we refer to the wet transition when less than 75% of profiles show wet coupling, but wet coupling is more common than any other coupling state.

3. Results

a. Observational results

Meteorological variables at the study site exhibited large seasonal cycles. From May through September, defined here as the convective season, T_{Air} increased from May to July and often exceeded 30°C around noon (Fig. 3). The annual and diurnal temperature cycle is closely associated with the behavior of the VPD, which also exhibited its largest magnitude in July at more than −40 hPa on average. Ecohydrological conditions at US-FPe were not only characterized by VPD, but also by annual dynamics of H and LE. While there was comparatively little variation in H between months, a clear pattern in average LE emerged. From May to June mean maximum daytime LE increased from approximately 125 to $175\,W\,m^{-2}$ and then decreased to $75\,W\,m^{-2}$ in September. Correspondingly, peak daytime Bo values decreased to below 1.0 on average from May to June and reach a maximum average Bo of approximately 2.5 in September. As required by the model, Bo was generally constant between 0800 and 1600 LT, that is, the typical timing of convective phenomena (Fig. 3e).

A look at quantiles of mean daytime Bo (Table 1) reveals that Bo can drop below 0.5 for a significant portion of days during June and July, whereas for the other months of the convective season Bo remained higher. At the upper end of the daytime Bo range, Bo values exceeding 2.75 made up more than 25% of days for all months except June.

The progressive summertime drying in northeastern Montana and the Fort Peck area are also evident in the precipitation data. Average precipitation at US-FPe decreased from more than $2\,mm\,day^{-1}$ in May to less than $1\,mm\,day^{-1}$ in September (not shown). Similarly the number of rain events also decreased.

As expected, θ increased with height ($\gamma_\theta > 0$), while q decreased ($\gamma_q < 0$) due to the surface moisture source and higher near-ground temperatures (Figs. 2a–d). Compared to γ_θ, which has a relatively even frequency between approximately 2 and $4\,K\,km^{-1}$, γ_q exhibits a clear peak around $1\,g\,kg^{-1}\,km^{-1}$, indicating higher variability for γ_θ. Nevertheless, γ_q can occasionally turn positive when surface conditions are very dry. Both γ_θ and γ_q show a clear cycle through the convective season reaching their respective minima in July. The coinciding decrease in stability and the increased vertical moisture gradient can preclude the development of boundary layer clouds and convection through entrainment of increasingly dry air into the ML, and it is important to investigate their interactions and relationship to surface conditions.

b. Climatological trends

To characterize climatological trends in the Fort Peck region, we proceed to analyze MERRA-2 reanalysis data (Fig. 4). Monthly mean data show significant increasing trends for LE from 2.8 to $7.2\,W\,m^{-2}\,decade^{-1}$ (at the $p < 0.05$ level, Table 2) since 1980. Trends were present during all months of the convective season, despite considerable year to year variation. At the same time, H decreased between −1.8 and $-4.5\,W\,m^{-2}\,decade^{-1}$, which is significant for June, August, and September. The net result is significant decreases in Bo between −0.21 and $-0.29\,decade^{-1}$ for all months, indicating increased moisture transfer from the surface to the ML. MERRA-2 does not exhibit significant trends for R_n. When comparing surface energy balance components from MERRA-2 to observations at US-FPe, it becomes apparent that while there is good agreement between mean LE estimates from MERRA-2 and measurements at US-FPe, MERRA-2 overestimates observed H by approximately 25% for most months of the convective season, such that MERRA-2 derived Bo appears to be underestimated. Interestingly, the disagreement in mean H is of similar magnitude to the discrepancy in R_n, where MERRA-2 values exceed US-FPe observations. Observed values at US-FPe exhibit larger year to year variability than MERRA-2 data (as seen from individual years in Fig. 4), which further complicates the comparison between local observations and reanalysis data and obscures local climatic trends in observations. Caution should be exercised when comparing globally gridded datasets, such as MERRA-2, to point observations because of assumptions and methodological limitations discussed in section 4b. Significant trends in LE and Bo are consistent with the notion of increasing near-surface moisture and coincide with a significant negative trend of γ_q during meteorological summer (JJA) derived from radiosonde profiles.

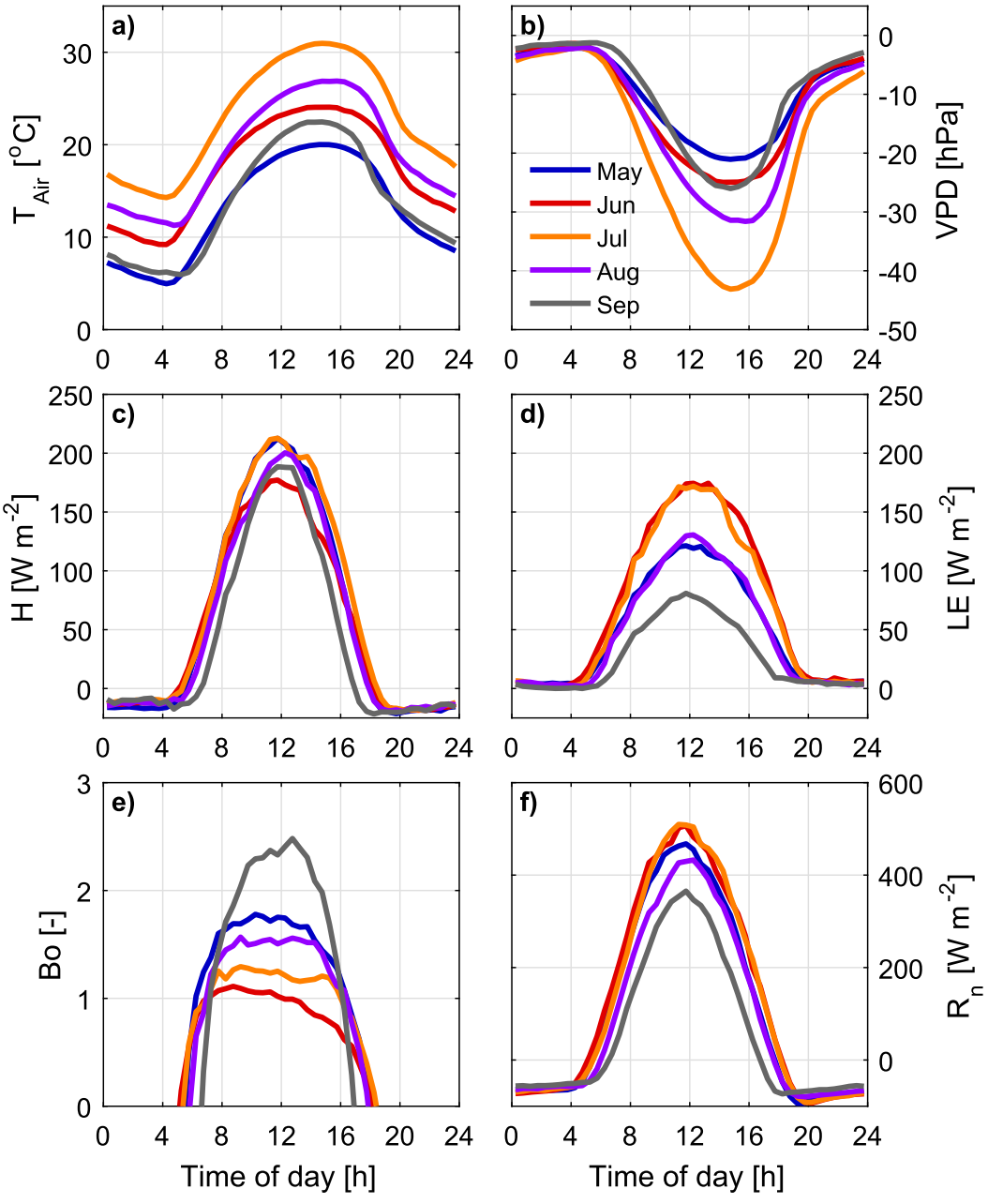

FIG. 3. The observed median diurnal cycle of (a) T_{Air}, (b) VPD, (c) H, (d) LE, (e) Bo, and (f) R_n for the May–September convective season at the US-FPe eddy covariance research site between 2000 and 2008.

Results for γ_θ were inconclusive because of large interannual variability and showed no consistent trends.

c. *Modeled h and LCL at US-FPe*

During the convective seasons of 2000–08, there were only 63 days (out of 561 days passing quality control) with recorded daytime precipitation at US-FPe, highlighting the dry conditions in northeastern Montana. Of these, 19 occurrences were on days when modeled h exceeded the LCL. Overall, and despite the simplifications discussed above, the model appears to mostly capture the timing of locally developing precipitation events (Fig. 5a). The two events where precipitation occurred more than 5 h after h crossing the LCL were individually identified as large-scale precipitation events. Subsequently, the model is used to test whether the different model outcomes described in section 2b correspond to differences in environmental and

TABLE 1. Statistics of $R_{n,\max}$ and Bo at US-FPe.

	$R_{n,\max}$ percentile (W m^{-2})					Bo percentile				
Month	10th	25th	50th	75th	90th	10th	25th	50th	75th	90th
May	271	451	546	597	640	0.68	1.06	1.81	2.86	4.70
Jun	366	540	592	641	697	0.36	0.57	0.91	1.48	3.61
Jul	483	517	550	598	630	0.38	0.53	1.16	3.26	7.81
Aug	393	434	475	512	553	0.51	0.74	1.36	2.91	7.28
Sep	244	336	380	424	465	0.79	1.34	2.98	6.72	11.56

atmospheric conditions, which is an important prerequisite for applying the model to study the sensitivity of the system to climatic and ecohydrological changes.

Results suggest (Figs. 5b–d) that the convective outcomes of the model show little dependence on γ_θ and γ_q, and rather depend on Bo and ML moisture contents for which $RH_{FA,0}$ (the relative humidity calculated from $\theta_{FA,0}$ and $q_{FA,0}$) is a proxy. Days for which h remains below the LCL are characterized by values of $RH_{FA,0} < 50\%$. At the same time, precipitation development for days with hxLCL is associated with lower Bo than days during which no precipitation occurs. The four model outcomes also separate with respect to their location within the CTP–HI_{low} framework (Fig. 5d). Instances without hxLCL are characterized by higher HI_{low} and thus dry atmospheric conditions that suppress convection.

Accepting that the model distinguishes between defined atmospheric and environmental states for locally developing convection, we frame our subsequent discussion in terms of the role of observed changes in regional hydrometeorological conditions on processes related to convective initiation.

4. Discussion

a. Observations

Observed seasonal patterns of LE and Bo (Fig. 3) can be used to characterize the ecohydrologic environment

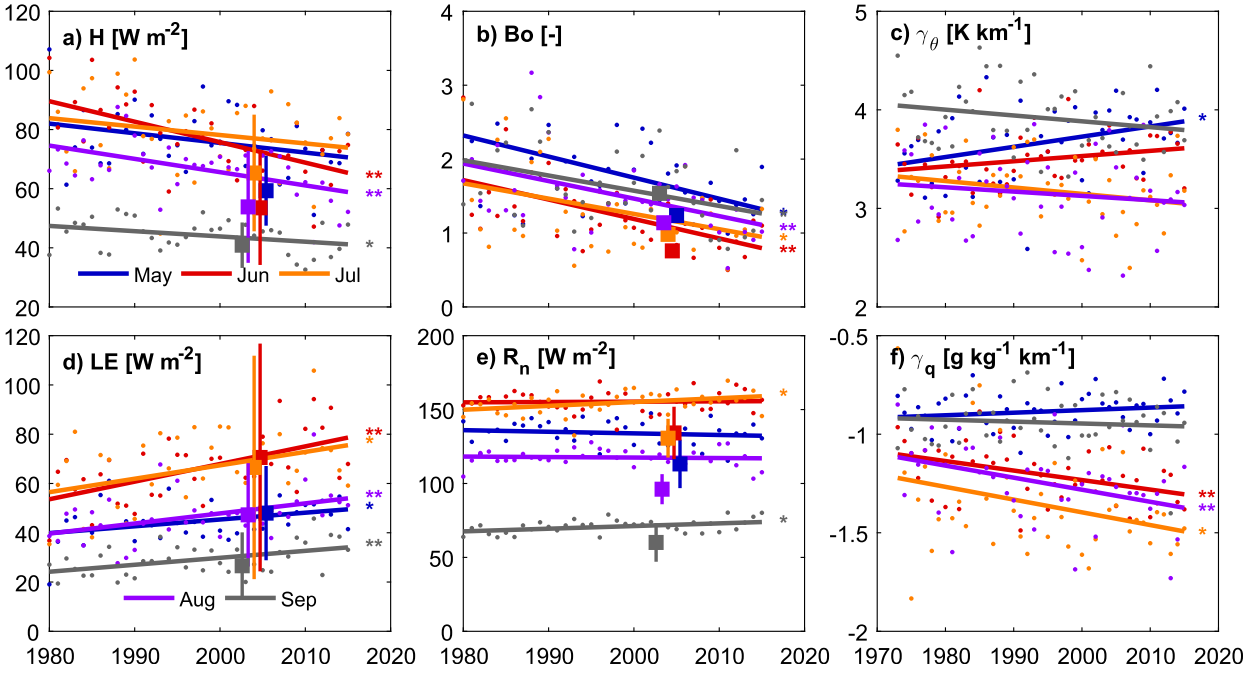

FIG. 4. Climatic surface trends for May–September (left),(center) from MERRA-2 for the US-FPe and (right) from radiosondes at GGW for (a) H, (b) Bo, (c) γ_θ, (d) LE, (e) R_n, and (f) γ_q. Lines represent a linear fit to monthly means (dots). The squares indicate observed values at US-FPe (mean) and their standard deviation (vertical bars). Significant trends are indicated by * ($p < 0.05$) and ** ($p < 0.01$).

TABLE 2. Linear trend and significance level (p value) for MERRA-2 surface variables at US-FPe for the period 1980–2015 and sounding lapse rates at GGW for the period 1973–2015.

	May		June		July		August		September	
Variable	Trend	p	Trend	p	Trend	p	Trend	p	Trend	p
H (W m^{-2} decade^{-1})	−3.26	0.053	−6.93	<0.001	−2.85	0.179	−4.49	0.001	−1.78	0.043
LE (W m^{-2} decade^{-1})	2.76	0.028	7.16	<0.001	5.45	0.021	4.09	0.010	2.83	0.004
R_n (W m^{-2} decade^{-1})	−1.08	0.417	0.22	0.844	2.60	0.028	−0.34	0.714	1.80	0.014
Bo (decade^{-1})	−0.29	0.018	−0.26	<0.001	−0.21	0.017	−0.24	0.003	−0.21	0.011
γ_θ (K km^{-1} decade^{-1})	0.10	0.021	0.05	0.095	−0.07	0.121	−0.04	0.412	−0.06	0.146
γ_q (g kg^{-1} km^{-1} decade^{-1})	0.01	0.258	−0.05	0.004	−0.06	0.036	−0.06	0.009	−0.01	0.547

at US-FPe. From May to June, plant development increased evapotranspiration. Then, from June until August the environment became increasingly drier, due in part to plant senescence (Vick et al. 2016), thus reducing LE and increasing the average Bo to approximately 2.5 in September. High VPD can rapidly decrease Bo in grasslands, which can exhibit isohydric behavior (i.e., maintain near constant leaf water potential) and close stomatal control over transpiration (Novick et al. 2016; Konings et al. 2017). The results highlight the interactions between vegetation, environmental drivers, and ecophysiological responses to the

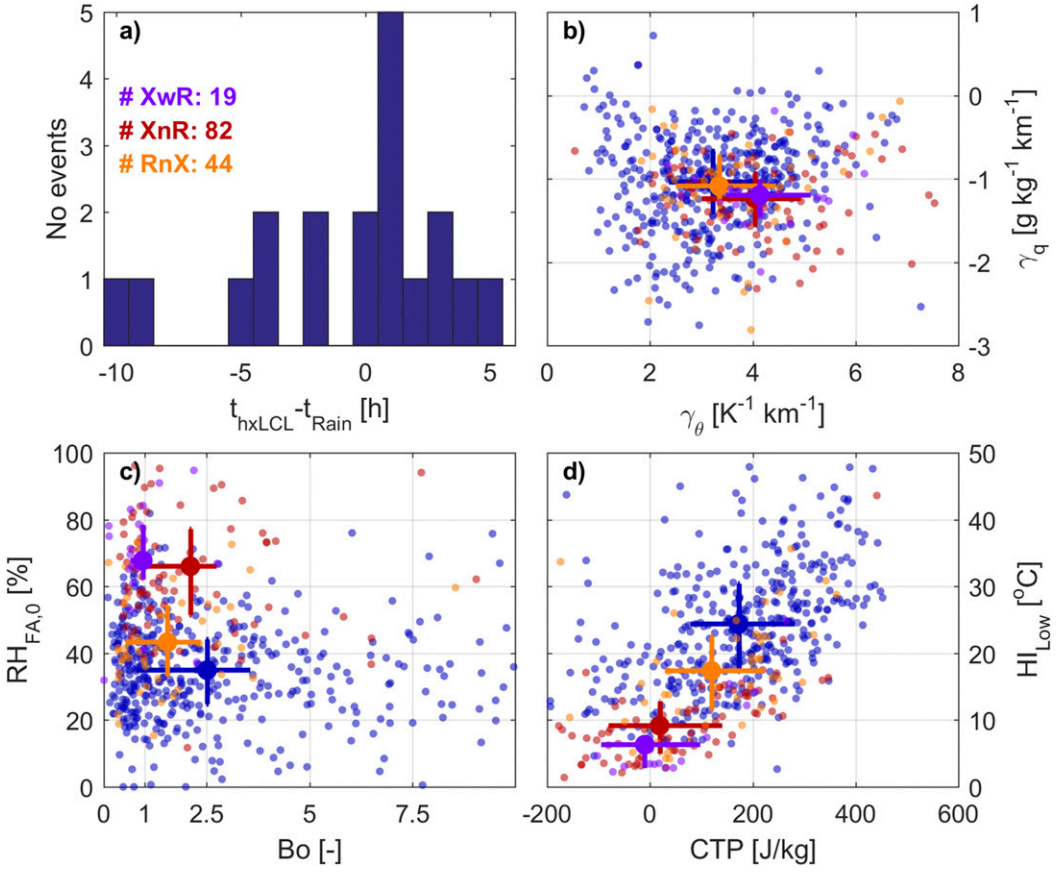

FIG. 5. Summary of daily ML model results using US-FPe observations as model forcing: (a) timing of modeled ABL height h crossing the LCL (i.e., hxLCL) compared to the observed start of precipitation and grouping of boundary layer states (explained in text) based on environmental conditions such as (b) temperature and moisture lapse rates, (c) effective ML relative humidity, and (d) CTP–HI_{low} framework for groups: no observed precipitation and $h_{max} < LCL$ (blue), observed precipitation and $h_{max} < LCL$ (orange, RnX), $h_{max} > LCL$ and no observed precipitation (red, XnR), and $h_{max} > LCL$ with precipitation (purple, XwR). The median and interquartile range for each group is indicated by the crosses.

land–atmosphere exchange of water, while the extremely high Bo values encountered during July–September demonstrate the frequently very dry surface conditions in the study area. The observed diurnal behavior of Bo is in reasonable agreement with the expectation of constant Bo during the daytime (Crago and Brutsaert 1996; Gentine et al. 2007, 2011), which is assumed by the ML model.

b. Climatological trends

Given that direct observations of surface energy balance and land–atmosphere exchange of energy and water are both labor intensive and expensive, their availability is inherently limited. To bridge this gap, this work applies MERRA-2 data, which are available from 1980 onward to assess climatic trends in the region (Figs. 4a–d). However, global gridded datasets such as MERRA-2 should be used with caution given that subgrid-scale surface heterogeneity, data assimilation, observational uncertainties, and the underlying modeling system cause local biases that affect water and energy cycles (e.g., Decker et al. 2012; Santanello et al. 2015). Nevertheless, in the absence of long-term observations, they can provide a first-order estimate of regional climatic trends, noting that the eddy-covariance site, which provides local measurements, might not be fully representative with respect to land cover, topography, or soil moisture of the MERRA-2 grid cell. Additionally, surface energy balance components in MERRA-2 are highly dependent on accurate prediction of local cloud cover, and MERRA-2 is demonstrated to have a positive bias in R_n due to cloud cover biases (Draper et al. 2018). The discrepancy in R_n between MERRA-2 and US-FPe, which is also reflected in H, suggests that cloud cover in MERRA-2, which (except for the Amazon basin; Marquardt Collow and Miller 2016) has not been assessed to date, might introduce a positive bias in R_n from MERRA-2 at the site. Similarly, the quality of reanalysis data is also affected by density and distribution of assimilated observations (e.g., Ferguson and Villarini 2012). While these limitations affect absolute values, moistening trends in MERRA-2 data are consistent with radiosonde observations (Fig. 4f) of increasing negative moisture lapse rates. However, the exact reason for the moistening trend is unclear and likely associated with both moistening of MLs due to increasing LE and changes to large-scale atmospheric moisture transport.

Betts et al. (2013, 2014) reported increasing cloud cover in agricultural regions of the Canadian Prairie provinces, which is consistent with higher downward longwave radiation and lower solar irradiance. While we find a comparatively small effect on R_n (Table 1), Betts et al. (2013, 2014) indicated an R_n reduction of some 6 W m^{-2}. Given the fact that the effect of cloud cover on R_n is both dependent on cloud type and time of day as well as the lack of a consistent trend in the MERRA-2 dataset, we limit our analysis of coupling effects between the surface and the atmosphere to surface energy partitioning (Bo) rather than energy input (R_n). Additionally, we focus on increased moistening of the lower troposphere rather than changes in stability based on the MERRA-2 data. Note that while the conducted analysis of climatological trends motivates our investigation of changes to wet and dry coupling behavior in the northern Great Plains, the analysis itself does not use MERRA-2 data and is therefore not affected by biases in the reanalysis.

c. Modeled h and LCL at US-FPe

The small portion of precipitating hxLCL events (Fig. 5) warrants discussion, as it might indicate overdetection of LCL crossings by the model. While misdetection of events cannot be fully excluded, note that summertime HI_{low} values are much higher than for previous studies (Findell and Eltahir 2003a,b), indicating that despite high observed H, the lack of low-level moisture in atmospheric profiles frequently controls convective development by suppressing the transition from shallow to precipitating convection, which is governed to a significant degree by the availability of moisture (Wu et al. 2009). For the sake of simplicity, the analytical model of Porporato (2009) is used in this work, which precludes the quantification of thermodynamic conditions under which the level of free convection is reached that require realistic profiles (Gerken et al. 2013) and can be assessed through integrated frameworks (see, e.g., Tawfik and Dirmeyer 2014; Tawfik et al. 2015). Also, eastward propagating mesoscale convective systems (MCSs) generated east of the Rocky Mountains (e.g., Tuttle and Davis 2006; Phillips and Klein 2014) are responsible for approximately 60% of total precipitation in the U.S. Great Plains (Carbone and Tuttle 2008). Because of their local nature, ML models, in general, cannot account for precipitation attributed to MCS, thus reducing the skill of the model to predict precipitation timing. This also limits direct feedbacks between local convection and soil moisture. However, because of the prevailing dryness in northeastern Montana, even moderate amounts of locally forced convective precipitation can be a crucial source of water for agriculture.

The ML model is used to assess environmental conditions governing the occurrence of hxLCL events and, furthermore, to establish whether certain environmental conditions are more likely to be associated with convective precipitation. Results demonstrate that both near-surface RH and Bo can be used to classify

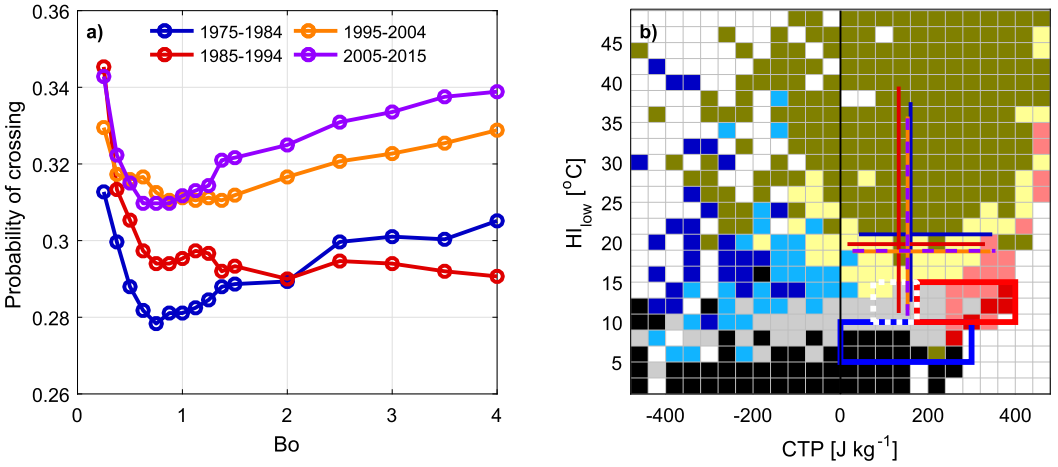

FIG. 6. Model-estimated wet–dry coupling (defined in text) for the 75th percentile of $R_{n,\max}$: (a) probability of hxLCL as a function of Bo and (b) coupling behavior visualized in CTP–HI$_{low}$ space. Blue and red areas are for wet and dry coupling. Black areas exhibit crossing behavior regardless of Bo, while olive areas do not exhibit crossings. Light red, blue, gray, and yellow indicate the transition zone between coupling states (see section 2d for details). The wet–dry coupling areas as proposed by Findell and Eltahir (2003a,b) are indicated by the colored rectangles, with red, blue, and white for dry, wet, and transitional coupling, respectively. The crosses in (b) show the median and interquartile range for radiosonde profiles for each decade.

convective states at US-FPe. The fact that precipitation development for days with hxLCL is associated with smaller Bo values than for hxLCL events without precipitation is consistent with the notion that for small Bo (~1) there is sufficient moisture supplied from the surface to the ML as to not impede the transition from shallow to precipitating clouds. Midlevel moisture and stability of the atmospheric profiles are also key components in governing the transition from shallow clouds to precipitation. The CTP–HI$_{low}$ framework can be used to explain the impact of atmospheric control on convection. Days without hxLCL are associated with high moisture deficits (high HI$_{low}$). As a consequence, CAPE as indicated by CTP cannot be released because of very high LCLs (often exceeding 4000 m; see also Vick et al. 2016). The fact that precipitation associated with hxLCL occurs at slightly lower CTPs compared to days without precipitation appears to be counterintuitive. However, note that CTP calculations are performed from the 1200 UTC soundings at GGW, which are measured before sunrise and in considerable distance to US-FPe, so that they may not perfectly match local conditions. Findell and Eltahir (2003a,b) discussed that the northern Great Plains (including GGW) was part of a transitional region with no clear dominance of atmospheric and surface control on convective triggering. Additionally, they assumed CTP $< 0\,\mathrm{J\,kg^{-1}}$ and HI$_{low} > 15$°C as thresholds suppressing convective precipitation. However, later studies using reanalysis data (Ferguson and Wood 2011; Roundy et al. 2013) found that the classes defined originally from radiosondes in Illinois (Findell and Eltahir 2003a,b) were too narrow to determine wet and dry coupling or atmospheric control over precipitation in different regions while still demonstrating the usefulness of the CTP–HI$_{low}$ framework. Atmospheric control on convection is discussed in more detail in sections 4d and 5.

d. *Wet and dry coupling*

The analysis of coupling regimes for GGW is broadly consistent with the results obtained by Findell and Eltahir (2003b). Figure 6a shows both wet and dry coupling behavior as indicated by the maximum of hxLCL probabilities for very low and very high Bo. At the same time, Fig. 6b reveals that the median state of the atmosphere is close to conditions where convection is suppressed mainly due to a lack of midlevel moisture, highlighting the role of atmospheric profiles in governing convective development near Fort Peck. Modeling results using the 75th percentile of $R_{n,\max}$ show a minimum for hxLCL at Bo ~ 1, which is close to the current average observed Bo at US-FPe. The existence of such a minimum indicates that both wet and dry coupling exist at US-FPe depending on atmospheric conditions. Reducing $R_{n,\max}$ to the 25th percentile did not considerably alter the wet–dry coupling behavior, but reduces the probability of hxLCL by approximately 0.05–0.08 (not shown), demonstrating that the finding is robust with respect to energy input. Atmospheric moistening during the last 40 years increased the probability of hxLCL events by approximately 10% (3–5 percentage points), which is most likely attributed to increased near-surface

TABLE 3. Statistics of observed CTP–HI_{low} from soundings at GGW.

Period	CTP percentile ($J\,kg^{-1}$)			HI_{low} percentile (°C)		
	25th	50th	75th	25th	50th	75th
1975–84	42.4	160.4	263.9	12.5	21.0	29.0
1985–94	16.0	133.3	243.7	11.1	19.8	29.8
1995–2004	28.1	153.7	257.3	11.5	18.8	27.5
2005–14	27.6	153.5	263.6	10.8	18.9	27.8

moisture. Noting that Bo values at US-FPe from MERRA-2 have decreased from approximately 2 to 1 over the last three to four decades (Fig. 4), it becomes apparent that both Bo and atmospheric profiles contributed to trends in coupling behavior, albeit with differences in sign as the decreasing Bo moved the system toward less convectively preconditioned states. However, the effects from the Bo reduction appear to be partially compensated by the shift of the LCL crossing minimum to smaller Bo (Fig. 6a). Interestingly, the majority of the change happened between the periods of 1975–84 and 1995–2004, while the period from 2005 to 2014 exhibited little additional change.

The coupling behavior and its relationship to atmospheric control are further illustrated with results from the CTP–HI_{low} framework (Fig. 6b). The median CTP–HI_{low} state observed at GGW is close to the boundary between atmospheric control preventing convective triggering and transitional states. Since 1975, median HI_{low} values have decreased by approximately 2°C, while trends in CTP were less clear (Table 3). As a consequence, coupling states moved from atmospheric control to a more transitional state. Note that despite using 40 years of sounding data (>6000 profiles), bins that correspond to CTP–HI_{low} combinations outside the interquartile range in Fig. 6b are sparsely populated or not populated by data, resulting in less clearly defined areas of coupling compared to Roundy et al. (2013), who used a much larger regional dataset. Nevertheless, compared to previous studies (Findell and Eltahir 2003b; Roundy et al. 2013), coupling behavior is found at more negative CTP values and higher HI_{low} values. Additionally, less defined areas of coupling also suggest that while the CTP–HI_{low} framework is useful to broadly characterize coupling, there are additional atmospheric factors that affect coupling behavior. Recent work by Cioni and Hohenegger (2017) showed that total precipitation amounts were always smaller during dry coupling compared to wet coupling, which is consistent with the notion that total column precipitable water rather than locally sourced moisture makes up the bulk of rainfall (e.g., Trenberth 1999). These issues suggest that modifications to the CTP–HI_{low} framework, which, given our focus on ML development is beyond the scope of this work, may help in better capturing convectively preconditioned states and resulting rainfall in northeastern Montana.

5. Sensitivity of land–atmosphere coupling to climatic trends

While the underlying cause of the climatic trends affecting northeastern Montana as a whole are unclear, trends in Bo, γ_q, and q over the last 40 years not only affect the mean state of these variables, but also have the potential to affect the frequency of convective clouds and precipitation due to surface–ABL coupling. A better understanding of past surface–atmosphere coupling behavior and inherent feedbacks can be used to inform potential future changes in response to both global and local change, which results from agricultural intensification (e.g., summer fallow reduction) or other shifts in cropping systems, like the adoption of no-till farming, which likewise affect atmospheric processes (Long et al. 2014; Luyssaert et al. 2014; Davin et al. 2014; Mueller et al. 2015; Vick et al. 2016; Bright et al. 2017).

The comparison between the modeled h and LCL using sounding profiles for the decades from 1975 to 1985 and from 2005 to 2015 reveals a considerable increase in likelihood of hxLCL (Fig. 7) for a given level of $R_{n,max}$. This analysis assumes no climatic trend in $R_{n,max}$, which appears reasonable based on the MERRA-2 data (Fig. 4), despite the fact that increasing surface moisture and land use change trends affect the surface albedo and thus R_n. However, R_n is governed to a large extent by cloud cover, which historically is sparsely recorded and strongly affected by subgrid-scale effects in reanalysis data. Betts et al. (2013) reported an increase in cloud cover and a corresponding decrease in R_n for weather stations in the Canadian Prairies, but as clouds affect both shortwave and longwave radiative transfer, the net effect of changes in cloud cover on R_n is not straightforward and depends also on timing of clouds as well as their structure, reconciling observations with the lack of clear trends in MERRA-2 data. Alternatively, there may be problems with the representation of cloud cover in MERRA-2.

Trends in Bo also affect convective outcomes by increasing the probability of hxLCL and thus likely convection (for constant $R_{n,max}$), which can be attributed to the trends in atmospheric profiles and near-surface levels of q. Between 1975–85 and 2005–15, average daily Bo from MERRA-2 for the pixel including US-FPe decreased by approximately 0.5 or more for most months of the convective season, moving observed Bo

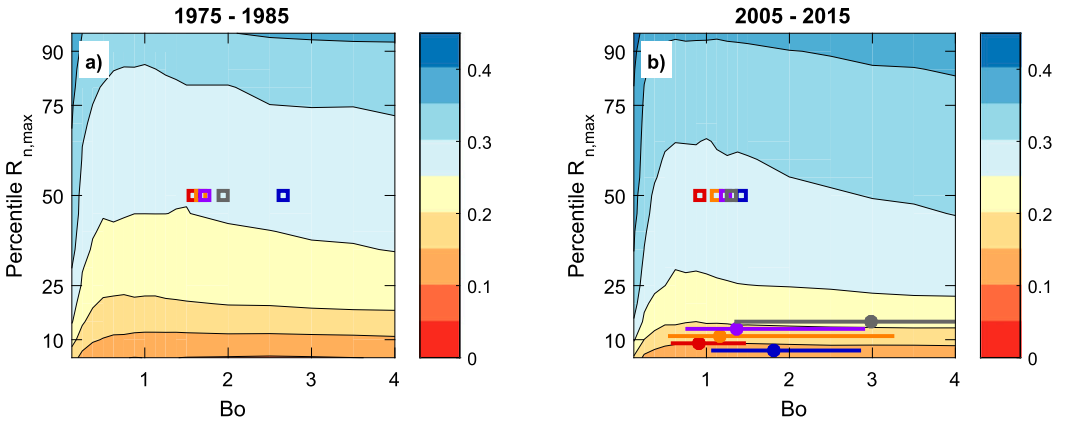

FIG. 7. Modeled wet–dry coupling behavior as a function of $R_{n,\max}$ and Bo for the decades (a) 1975–85 and (b) 2005–15. Contour lines indicate probability of hxLCL events. Squares indicate the mean monthly Bo from MERRA-2 for May–September (blue, red, orange, purple, and gray, respectively). Note that MERRA-2 data start in 1980. Colored circles and error bars indicate median and interquartile range of observed mean daytime Bo at US-FPe. See Table 1 for values of $R_{n,\max}$ and Bo.

closer to the area of high Bo sensitivity, which is characterized by a sharp increase in the probability of convective outcomes (Fig. 7). In contrast, Bo values during 1975–85 (Bo ≈ 1.5–2.5) were in a much less Bo-sensitive region. These findings are also highlighted by the eddy-covariance-derived distribution of mean daytime Bo. Especially during June and July, the 10th and 25th percentiles of Bo reach into the region of high hxLCL sensitivity. As a consequence, a combination of trends in Bo, γ_q, and q are likely responsible for changes in convective cloud formation at US-FPe. Given the full monthly distribution of Bo, it is likely that any further shift in the Bo distribution might be associated with an increase in convective outcomes. Our results are consistent with Dirmeyer et al. (2014), who showed that projected climate trends increase feedbacks between the land surface and ABL. However, given the prevailing change of CTP and $\mathrm{HI_{low}}$ in the atmospheric profiles between 1975 and 2005, rather than the past decade, ongoing monitoring is needed to find out whether this constitutes a pause or a more systematic shift in climatic trends, noting as well that the precise domain of surface and atmospheric change across the U.S. northern Great Plains has yet to be defined (Fig. 1).

There is also strong seasonal behavior in the environmental controls governing convectively preconditioned conditions as revealed by $q_{\mathrm{FA},0}$, γ_q, and Bo. The hxLCL results from the interplay between ML growth and moisture mixing ratios inside the ML, which is governed by initial moisture ($\sim q_{\mathrm{FA},0}$), dry air entrainment across the ML top ($\sim\gamma_q$), and moisture supply (Bo) through partitioning of R_n into LE and H. As greater H increases ML growth at the expense of the moisture flux into the ML through LE, and less negative vertical moisture lapse rates decrease the drying of the ML during its growth, hxLCL can be achieved both by growing h to reach the LCL and by decreasing the LCL to reach h through the moistening of the ML (Juang et al. 2007a,b). The results show that these relationships exhibit behavior that varies considerably throughout the convective season, resulting in a reversal in the Bo sensitivity from May to September (Fig. 8).

In May during the beginning of the convective season, the boundary between modeled convective and non-convective behavior is located within the interquartile range of atmospheric moisture characteristics. At the same time, the system shows a moderate to weak sensitivity with respect to Bo, where larger Bo requires higher $q_{\mathrm{FA},0}$ for convection to develop. This signifies that during times with comparatively low LCLs it is "easier" to reach the convectively preconditioned state by moistening the ML, rather than by partitioning energy toward h growth. In June the system is in a transitional state between wet and dry coupling, with the consequence that sensitivity to Bo is low. Similar to May, convectively preconditioned states can frequently be reached as atmospheric characteristics are close to the hxLCL boundary. In July and August, the LCL tends to be higher so that LCLs exceeding 3–4 km are common (e.g., Vick et al. 2016). As a consequence, rapid ML growth through high Bo is more advantageous and hxLCL is controlled thermodynamically (Gentine et al. 2013a) rather than dynamically through atmospheric moisture content. At the same time, higher $R_{n,\max}$ and decreasing γ_q indicate that the system is becoming less energy limited and more moisture limited.

The notion that moisture limitation is a limiting factor in convection development is supported by the

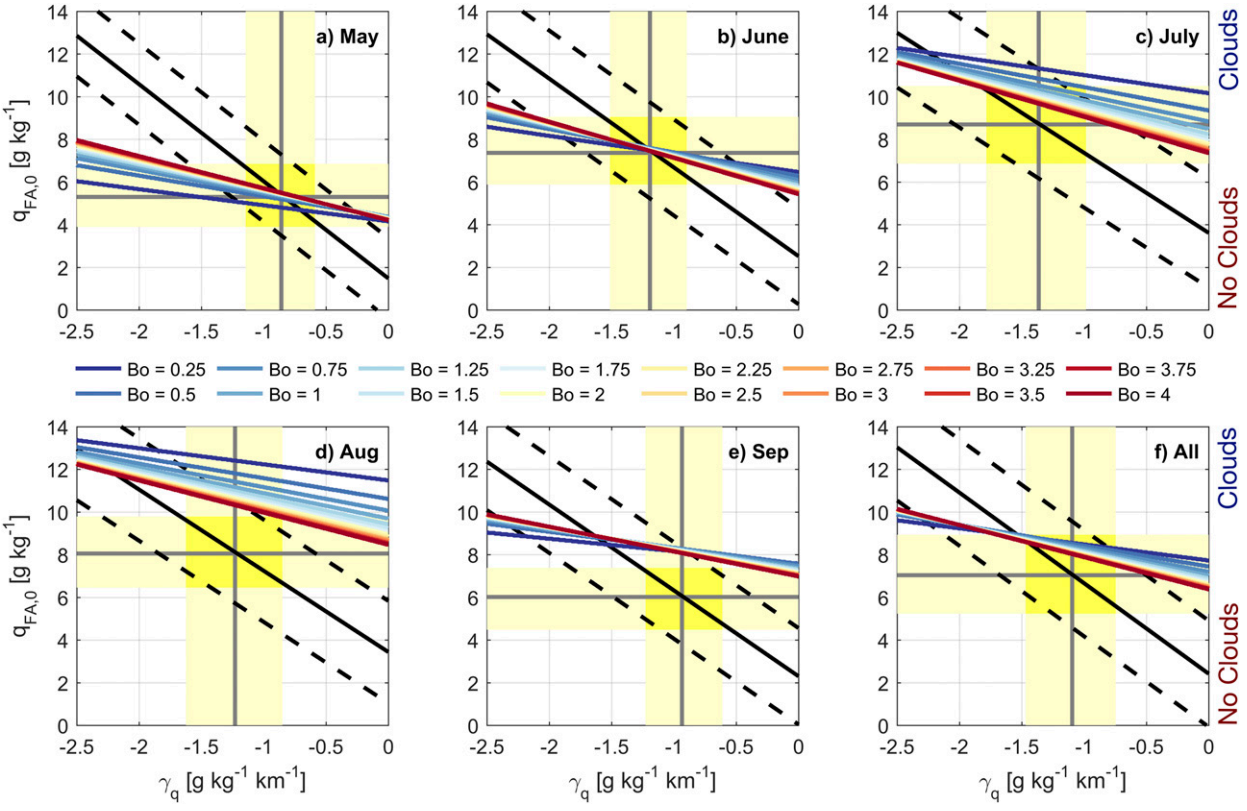

FIG. 8. Modeled sensitivity of hxLCL for (a)–(e) May–September and (f) the complete May–September convective season. The colored lines indicate the dividing line between clouds and no clouds for the range of Bo from 0.25 to 4.0. Initial conditions corresponding to $q_{FA,0}$ and γ_q above the Bo line will lead to clouds at a given Bo, while initial conditions below the lines remain cloudless. Yellow patches indicate the interquartile range of observed radiosonde profiles from GGW, with the gray lines indicating the median state. The black line shows the observed correlation between $q_{FA,0}$ and γ_q, with a 95% confidence interval (dashed black lines). The analysis assumes initial clear sky conditions with $R_{n,max}$ corresponding to the 90th percentile and mean atmospheric stability γ_θ.

comparison between observed distributions of γ_q and $q_{FA,0}$ to the thresholds for hxLCL. During May and June the threshold for the range of observed Bo is not only within the interquartile range of γ_q and $q_{FA,0}$, but also touches the median state (Fig. 8). Later during the convective season and especially in July and August, however, the lines for the convective threshold move toward higher $q_{FA,0}$, so that convectively preconditioned atmospheric states become rare. Note that while $q_{FA,0}$ increases from May to July, it is RH (which is also a function of T and P) rather than q that determines the LCL, and temperatures at US-FPe rise rapidly between May and July from approximately 20° to 30°C around noon (Fig. 3a). The Bo sensitivity reaches its maximum in August and then declines toward September and the end of the convective season. At the same time, the system becomes increasingly more moisture limited as convectively preconditioned conditions for all but extremely high Bo are outside the interquartile range of observed γ_q and $q_{FA,0}$.

This behavior agrees well with observed precipitation events in August and September at US-FPe, which are rare compared to rain events earlier in the season (results not shown) and the finding of reduced modeled total precipitation during dry coupling (Cioni and Hohenegger 2017). Last, the strong seasonality of behavior between May and September highlights the fact that the sensitivity between atmospheric moisture and energy partitioning should be examined on a subseasonal/monthly basis rather than for the convective season as a whole, since the season aggregated results (Fig. 8f) are greatly different from monthly results (Figs. 8a–e).

Our results suggest that convective precipitation occurs in northeastern Montana in response to atmospheric moistening and is becoming increasingly sensitive to Bo. Note the caveat that we assume convective precipitation, which we cannot assess directly, to behave like hxLCL following the notion that hxLCL is a ''necessary but not sufficient condition'' for convective

initiation. The Bo tends to decrease throughout the convective season, whereas wet and dry coupling shifts from wet toward dry coupling in the late summer. In September, the absence of convection is governed by dry atmospheric profiles (atmospheric control). The corresponding hydrometeorological response to climate trends is thus likely increasing convective precipitation in the earlier growing season, but less in late summer.

While the results of one-dimensional models are useful to explore land–atmosphere coupling, it should be noted that only local effects are taken into account. Nonlocal precipitation events, for example, through eastward propagating MCSs (Phillips and Klein 2014; Carbone and Tuttle 2008; Tuttle and Davis 2006), cannot be addressed with this method. Also, it is well known that mesoscale circulations (e.g., forced from thermal or soil moisture differences) are associated with convective triggering over dry patches (e.g., Taylor et al. 2007; Garcia-Carreras et al. 2010), affecting land–atmosphere coupling as described by Koster et al. (2004), Seneviratne et al. (2010), and others. Similarly, cloud development impacts surface processes through cloud shading (e.g., Lohou and Patton 2014; Gronemeier et al. 2017) and boundary layer development through dynamic and radiative effects (e.g., Stull 1988). It is therefore desirable to merge local and regional methods, as done in Song et al. (2016), to investigate land–atmosphere coupling from the local to the regional scale, and to define the region of the North American northern Great Plains that has undergone regional climate responses that are consistent with shifts in agricultural management (Gameda et al. 2007; Betts et al. 2013, 2014; Mahmood et al. 2014).

6. Conclusions

This work applies a simplified analytical model of mixed layer heights and the lifting condensation level combined with the CTP–HI_{low} framework (Findell and Eltahir 2003a,b) to northeastern Montana, a region that has undergone considerable land cover change (Long et al. 2014). Motivated by documented climatic changes over the past four decades—namely, higher near-surface moisture amounts and increased partitioning of net radiation to latent heat fluxes at the expense of sensible heat as evidenced by smaller Bowen ratios—we examine how these trends affect coupling behavior.

Based on precipitation timing and the fact that the four convective outcomes [defined as 1) nonconvection permitting and no precipitation, 2) large-scale precipitation not controlled by local effects, 3) convection permitting without rain, and 4) convection permitting and precipitating] could be separated based on model initial conditions and the thermodynamic state of the atmospheres as characterized by the CTP–HI_{low} framework, the model is deemed to be useful to investigate the sensitivities of the system. However, CTP–HI_{low} alone cannot fully explain wet and dry coupling, suggesting that additional metrics are needed. Also, the very dry atmospheric conditions in August and September (suggesting atmospheric control on convection) and the small number of locally developed daytime precipitation events pose challenges to the modeling strategy yet emphasize the importance of additional convective season precipitation events to agricultural management. While mesoscale convective systems may be responsible for more than half of the total precipitation at Fort Peck, any additional precipitation from locally developing convection is likely to have a beneficial impact on crop yields.

Convectively preconditioned conditions near Fort Peck are closely associated with the availability of atmospheric moisture and sensible heat fluxes. Depending on tropospheric moisture contents and surface energy flux partitioning, mixed layer growth and associated entrainment of dry air can prevent the mixed layer height from reaching the LCL, while given adequate moisture supply, increased sensible heat fluxes are beneficial to reaching a convectively preconditioned state. As a consequence, the probability for convectively preconditioned conditions is smallest for intermediate Bowen ratios between approximately 0.5 and 2, indicating the presence of both wet and dry coupling. It is noteworthy that convectively preconditioned conditions occur at much drier conditions than proposed by Findell and Eltahir (2003a,b) and that the median state of the atmosphere is near the intersection point between moisture-limited suppressed convection as well as wet and dry coupling, highlighting the interplay between surface and atmospheric controls, which also exhibit seasonal dynamics. Over the course of the convective season the atmosphere transitions from wet coupling over dry coupling to atmospheric control, so that climatic trends suggest increased precipitation earlier in the season and less precipitation later on (August–September). At the same time, overall more convection is expected in response to regional moistening.

In the light of the climatic trend toward increased atmospheric moisture levels in the North American Great Plains (Pan et al. 2004) and the Great Plains' importance to agricultural production, increased understanding of land–atmosphere coupling can help devise strategies for improved land management or climate adaptation. Future studies should quantify the area undergoing these changes in both surface and atmospheric dynamics and quantify how ongoing changes in agricultural management have and perhaps will

continue to increase the likelihood of convective precipitation as approximated by mixed layer height and lifting condensation level crossings.

Acknowledgments. We acknowledge the Global Modeling and Assimilation Office (GMAO) and the GES DISC for the dissemination of MERRA. Funding for AmeriFlux data resources was provided by the U.S. Department of Energy's Office of Science. CTP is calculated using the *ctp_hi_low* function made public by A.B. Tawfik (coupling-metrics.com; github.com/abtawfik/coupling-metrics.git). The University of Wyoming's Atmospheric Science program and Larry Oolman are acknowledged for providing access to the radiosonde data (http://weather.uwyo.edu/upperair/sounding.html). We thank Tilden Meyer for eddy covariance data provision, and the AmeriFlux Management Project with the support of CDIAC for its harmonization. We acknowledge support from the National Science Foundation (NSF) Office of Integrated Activities (OIA) 1632810, the NSF Division of Environmental Biology (DEB) 1552976, the U.S. Department of Agriculture (USDA) National Institute of Food and Agriculture (NIFA) Hatch project 228396, the Montana Wheat and Barley Committee, and the graduate school at Montana State University. The authors thank Pierre Gentine and two anonymous reviewers for their helpful advice.

REFERENCES

Betts, A. K., R. Desjardins, D. Worth, and D. Cerkowniak, 2013: Impact of land use change on the diurnal cycle climate of the Canadian Prairies. *J. Geophys. Res. Atmos.*, **118**, 11 996–12 011, https://doi.org/10.1002/2013JD020717.

——, ——, ——, and B. Beckage, 2014: Climate coupling between temperature, humidity, precipitation, and cloud cover over the Canadian Prairies. *J. Geophys. Res. Atmos.*, **119**, 13 305–13 326, https://doi.org/10.1002/2014JD022511.

Bonetti, S., G. Manoli, J.-C. Domec, M. Putti, M. Marani, and G. G. Katul, 2015: The influence of water table depth and the free atmospheric state on convective rainfall predisposition: Water table and convective rainfall. *Water Resour. Res.*, **51**, 2283–2297, https://doi.org/10.1002/2014WR016431.

Bright, R. M., E. Davin, T. O'Halloran, J. Pongratz, K. Zhao, and A. Cescatti, 2017: Local temperature response to land cover and management change driven by non-radiative processes. *Nat. Climate Change*, **7**, 296–302, https://doi.org/10.1038/nclimate3250.

Brimelow, J. C., J. M. Hanesiak, and W. R. Burrows, 2011: Impacts of land atmosphere feedbacks on deep, moist convection on the Canadian Prairies. *Earth Interact.*, **15**, https://doi.org/10.1175/2011EI407.1.

Carbone, R. E., and J. D. Tuttle, 2008: Rainfall occurrence in the U.S. warm season: The diurnal cycle. *J. Climate*, **21**, 4132–4146, https://doi.org/10.1175/2008JCLI2275.1.

Cioni, G., and C. Hohenegger, 2017: Effect of soil moisture on diurnal convection and precipitation in large-eddy simulations. *J. Hydrometeor.*, **18**, 1885–1903, https://doi.org/10.1175/JHM-D-16-0241.1.

Crago, R., and W. Brutsaert, 1996: Daytime evaporation and the self-preservation of the evaporative fraction and the Bowen ratio. *J. Hydrol.*, **178**, 241–255, https://doi.org/10.1016/0022-1694(95)02803-X.

Davin, E. L., S. I. Seneviratne, P. Ciais, A. Olioso, and T. Wang, 2014: Preferential cooling of hot extremes from cropland albedo management. *Proc. Natl. Acad. Sci. USA*, **111**, 9757–9761, https://doi.org/10.1073/pnas.1317323111.

Decker, M., M. A. Brunke, Z. Wang, K. Sakaguchi, X. Zeng, and M. G. Bosilovich, 2012: Evaluation of the reanalysis products from GSFC, NCEP, and ECMWF using flux tower observations. *J. Climate*, **25**, 1916–1944, https://doi.org/10.1175/JCLI-D-11-00004.1.

Dirmeyer, P. A., Z. Wang, M. J. Mbuh, and H. E. Norton, 2014: Intensified land surface control on boundary layer growth in a changing climate. *Geophys. Res. Lett.*, **41**, 1290–1294, https://doi.org/10.1002/2013GL058826.

Draper, C. S., R. H. Reichle, and R. D. Koster, 2018: Assessment of MERRA-2 land surface energy flux estimates. *J. Climate*, **31**, 671–691, https://doi.org/10.1175/JCLI-D-17-0121.1.

Driedonks, A. G. M., 1982: Models and observations of the growth of the atmospheric boundary layer. *Bound.-Layer Meteor.*, **23**, 283–306, https://doi.org/10.1007/BF00121117.

Ek, M. B., and A. M. Holtslag, 2004: Influence of soil moisture on boundary layer cloud development. *J. Hydrometeor.*, **5**, 86–99, https://doi.org/10.1175/1525-7541(2004)005<0086:IOSMOB>2.0.CO;2.

Ferguson, C. R., and E. F. Wood, 2011: Observed land–atmosphere coupling from satellite remote sensing and reanalysis. *J. Hydrometeor.*, **12**, 1221–1254, https://doi.org/10.1175/2011JHM1380.1.

——, and G. Villarini, 2012: Detecting inhomogeneities in the Twentieth Century Reanalysis over the central United States. *J. Geophys. Res.*, **117**, D05123, https://doi.org/10.1029/2011JD016988.

Findell, K. L., and E. A. B. Eltahir, 2003a: Atmospheric controls on soil moisture-boundary layer interactions. Part I: Framework development. *J. Hydrometeor.*, **4**, 552–569, https://doi.org/10.1175/1525-7541(2003)004<0552:ACOSML>2.0.CO;2.

——, and ——, 2003b: Atmospheric controls on soil moisture-boundary layer interactions. Part II: Feedbacks within the continental United States. *J. Hydrometeor.*, **4**, 570–583, https://doi.org/10.1175/1525-7541(2003)004<0570:ACOSML>2.0.CO;2.

Ford, T. W., A. D. Rapp, and S. M. Quiring, 2015: Does afternoon precipitation occur preferentially over dry or wet soils in Oklahoma? *J. Hydrometeor.*, **16**, 874–888, https://doi.org/10.1175/JHM-D-14-0005.1.

Gameda, S., B. Qian, C. Campbell, and R. Desjardins, 2007: Climatic trends associated with summerfallow in the Canadian Prairies. *Agric. For. Meteor.*, **142**, 170–185, https://doi.org/10.1016/j.agrformet.2006.03.026.

Garcia-Carreras, L., D. J. Parker, C. M. Taylor, C. E. Reeves, and J. G. Murphy, 2010: Impact of mesoscale vegetation heterogeneities on the dynamical and thermodynamic properties of the planetary boundary layer. *J. Geophys. Res.*, **115**, D03102, https://doi.org/10.1029/2009JD012811.

Gelaro, R., and Coauthors, 2017: The Modern-Era Retrospective Analysis for Research and Applications, version 2 (MERRA-2). *J. Climate*, **30**, 5419–5454, https://doi.org/10.1175/JCLI-D-16-0758.1.

Gentine, P., D. Entekhabi, A. Chehbouni, G. Boulet, and B. Duchemin, 2007: Analysis of evaporative fraction diurnal

behaviour. *Agric. For. Meteor.*, **143**, 13–29, https://doi.org/10.1016/j.agrformet.2006.11.002.

——, ——, and J. Polcher, 2011: The diurnal behavior of evaporative fraction in the soil–vegetation–atmospheric boundary layer continuum. *J. Hydrometeor.*, **12**, 1530–1546, https://doi.org/10.1175/2011JHM1261.1.

——, C. R. Ferguson, and A. A. M. Holtslag, 2013a: Diagnosing evaporative fraction over land from boundary-layer clouds. *J. Geophys. Res. Atmos.*, **118**, 8185–8196, https://doi.org/10.1002/jgrd.50416.

——, A. A. M. Holtslag, F. D'Andrea, and M. Ek, 2013b: Surface and atmospheric controls on the onset of moist convection over land. *J. Hydrometeor.*, **14**, 1443–1462, https://doi.org/10.1175/JHM-D-12-0137.1.

Gerken, T., W. Babel, F. Sun, M. Herzog, Y. Ma, T. Foken, and H.- F. Graf, 2013: Uncertainty in atmospheric profiles and its impact on modeled convection development at Nam Co Lake, Tibetan Plateau. *J. Geophys. Res. Atmos.*, **118**, 12 317–12 331, https://doi.org/10.1002/2013JD020647.

Gronemeier, T., F. Kanani-Shring, and S. Raasch, 2017: Do shallow cumulus clouds have the potential to trigger secondary circulations via shading? *Bound.-Layer Meteor.*, **162**, 143–169, https://doi.org/10.1007/s10546-016-0180-7.

Guillod, B. P., B. Orlowsky, D. G. Miralles, A. J. Teuling, and S. I. Seneviratne, 2015: Reconciling spatial and temporal soil moisture effects on afternoon rainfall. *Nat. Commun.*, **6**, 6443, https://doi.org/10.1038/ncomms7443.

Harris, I., P. Jones, T. Osborn, and D. Lister, 2014: Updated high-resolution grids of monthly climatic observations the CRU TS3.10 dataset. *Int. J. Climatol.*, **34**, 623–642, https://doi.org/10.1002/joc.3711.

Juang, J.-Y., G. G. Katul, A. Porporato, P. C. Stoy, M. S. Siqueira, M. Detto, H.-S. Kim, and R. Oren, 2007a: Eco-hydrological controls on summertime convective rainfall triggers. *Global Change Biol.*, **13**, 887–896, https://doi.org/10.1111/j.1365-2486.2007.01315.x.

——, A. Porporato, P. C. Stoy, M. S. Siqueira, A. C. Oishi, M. Detto, H.-S. Kim, and G. G. Katul, 2007b: Hydrologic and atmospheric controls on initiation of convective precipitation events. *Water Resour. Res.*, **43**, W03421, https://doi.org/10.1029/2006WR004954.

Konings, A. G., G. G. Katul, and A. Porporato, 2010: The rainfall-no rainfall transition in a coupled land-convective atmosphere system. *Geophys. Res. Lett.*, **37**, L14401, https://doi.org/10.1029/2010GL043967.

——, S. C. Dekker, M. Rietkerk, and G. G. Katul, 2011: Drought sensitivity of patterned vegetation determined by rainfall-land surface feedbacks. *J. Geophys. Res.*, **116**, G04008, https://doi.org/10.1029/2011JG001748.

——, A. P. Williams, and P. Gentine, 2017: Sensitivity of grassland productivity to aridity controlled by stomatal and xylem regulation. *Nat. Geosci.*, **10**, 284–288, https://doi.org/10.1038/ngeo2903.

Körner, C., 1995: Leaf diffusive conductances in the major vegetation types of the globe. *Ecophysiology of Photosynthesis*, E.-D. Schulze and M. M. Caldwell, Eds., Springer Study Edition, Vol. 100, Springer, 463–490, https://doi.org/10.1007/978-3-642-79354-7_22.

Koster, R. D., and Coauthors, 2004: Regions of strong coupling between soil moisture and precipitation. *Science*, **305**, 1138–1140, https://doi.org/10.1126/science.1100217.

Kustas, W. P., T. J. Schmugge, K. S. Humes, T. J. Jackson, R. Parry, M. A. Weltz, and M. S. Moran, 1993: Relationships between evaporative fraction and remotely sensed vegetation index and microwave brightness temperature for semiarid rangelands. *J. Appl. Meteor.*, **32**, 1781–1790, https://doi.org/10.1175/1520-0450(1993)032<1781:RBEFAR>2.0.CO;2.

Lasslop, G., M. Reichstein, D. Papale, A. D. Richardson, A. Arneth, A. Barr, P. Stoy, and G. Wohlfahrt, 2010: Separation of net ecosystem exchange into assimilation and respiration using a light response curve approach: Critical issues and global evaluation. *Global Change Biol.*, **16**, 187–208, https://doi.org/10.1111/j.1365-2486.2009.02041.x.

Lohou, F., and E. G. Patton, 2014: Surface energy balance and buoyancy response to shallow cumulus shading. *J. Atmos. Sci.*, **71**, 665–682, https://doi.org/10.1175/JAS-D-13-0145.1.

Long, J. A., R. L. Lawrence, P. R. Miller, L. A. Marshall, and M. C. Greenwood, 2014: Adoption of cropping sequences in northeast Montana: A spatio-temporal analysis. *Agric. Ecosyst. Environ.*, **197**, 77–87, https://doi.org/10.1016/j.agee.2014.07.022.

Lubowski, R. N., M. Vesterby, S. Bucholtz, A. Baez, and M. J. Robterts, 2006: Major uses of land in the United States, 2002. USDA Economic Information Bulletin 14, 47 pp., https://www.ers.usda.gov/webdocs/publications/43967/13011_eib14_1_.pdf?v=42061.

Luyssaert, S., and Coauthors, 2014: Land management and land-cover change have impacts of similar magnitude on surface temperature. *Nat. Climate Change*, **4**, 389–393, https://doi.org/10.1038/nclimate2196.

Lytinska, Z., J. Parfiniewicz, and H. Piwkowski, 1976: The prediction of air mass thunderstorms and hails. *Proc. WMO Symp. on the Interpretation of Broad-Scale NWP Product for Local Forecasting Purposes*, WMO/TD-450, Warsaw, Poland, WMO, 128–130.

Mahmood, R., and Coauthors, 2014: Land cover changes and their biogeophysical effects on climate. *Int. J. Climatol.*, **34**, 929–953, https://doi.org/10.1002/joc.3736.

Manoli, G., J.-C. Domec, K. Novick, A. C. Oishi, A. Noormets, M. Marani, and G. Katul, 2016: Soil–plant–atmosphere conditions regulating convective cloud formation above southeastern US pine plantations. *Global Change Biol.*, **22**, 2238–2254, https://doi.org/10.1111/gcb.13221.

Marquardt Collow, A. B., and M. A. Miller, 2016: The seasonal cycle of the radiation budget and cloud radiative effect in the Amazon rain forest of Brazil. *J. Climate*, **29**, 7703–7722, https://doi.org/10.1175/JCLI-D-16-0089.1.

McPherson, R. A., D. J. Stensrud, and K. C. Crawford, 2004: The impact of Oklahoma's winter wheat belt on the mesoscale environment. *Mon. Wea. Rev.*, **132**, 405–421, https://doi.org/10.1175/1520-0493(2004)132<0405:TIOOWW>2.0.CO;2.

Meyers, T., 2000: AmeriFlux US-FPe Fort Peck. AmeriFlux, accessed 23 September 2016, https://doi.org/10.17190/AMF/1246053.

Mueller, N. D., E. E. Butler, K. A. McKinnon, A. Rhines, M. Tingley, N. M. Holbrook, and P. Huybers, 2015: Cooling of US Midwest summer temperature extremes from cropland intensification. *Nat. Climate Change*, **6**, 317–322, https://doi.org/10.1038/nclimate2825.

Novick, K. A., and Coauthors, 2016: The increasing importance of atmospheric demand for ecosystem water and carbon fluxes. *Nat. Climate Change*, **6**, 1023–1027, https://doi.org/10.1038/nclimate3114.

Oren, R., J. S. Sperry, G. G. Katul, D. E. Pataki, B. E. Ewers, N. Phillips, and K. V. R. Schäfer, 1999: Survey and synthesis of intra- and interspecific variation in stomatal sensitivity to vapour pressure deficit. *Plant Cell Environ.*, **22**, 1515–1526, https://doi.org/10.1046/j.1365-3040.1999.00513.x.

Pan, Z., R. W. Arritt, E. S. Takle, W. J. Gutowski, C. J. Anderson, and M. Segal, 2004: Altered hydrologic feedback in a warming climate introduces a warming hole. *Geophys. Res. Lett.*, **31**, L17109, https://doi.org/10.1029/2004GL020528.

Phillips, T. J., and S. A. Klein, 2014: Land-atmosphere coupling manifested in warm-season observations on the U.S. Southern Great Plains. *J. Geophys. Res. Atmos.*, **119**, 509–528, https://doi.org/10.1002/2013JD020492.

Porporato, A., 2009: Atmospheric boundary-layer dynamics with constant Bowen ratio. *Bound.-Layer Meteor.*, **132**, 227–240, https://doi.org/10.1007/s10546-009-9400-8.

Raddatz, R. L., 1993: Prairie agroclimate boundary-layer model: A simulation of the atmosphere/crop-soil interface. *Atmos.–Ocean*, **31**, 399–419, https://doi.org/10.1080/07055900.1993.9649478.

——, 2007: Evidence for the influence of agriculture on weather and climate through the transformation and management of vegetation: Illustrated by examples from the Canadian Prairies. *Agric. For. Meteor.*, **142**, 186–202, https://doi.org/10.1016/j.agrformet.2006.08.022.

Reichle, R. H., C. S. Draper, Q. Liu, M. Girotto, S. P. P. Mahanama, R. D. Koster, and G. J. M. De Lannoy, 2017: Assessment of MERRA-2 land surface hydrology estimates. *J. Climate*, **30**, 2937–2960, https://doi.org/10.1175/JCLI-D-16-0720.1.

Rienecker, M. M., and Coauthors, 2011: MERRA: NASAs Modern-Era Retrospective Analysis for Research and Applications. *J. Climate*, **24**, 3624–3648, https://doi.org/10.1175/JCLI-D-11-00015.1.

Rigby, J. R., J. Yin, J. D. Albertson, and A. Porporato, 2015: Approximate analytical solution to diurnal atmospheric boundary-layer growth under well-watered conditions. *Bound.-Layer Meteor.*, **156**, 73–89, https://doi.org/10.1007/s10546-015-0018-8.

Roundy, J. K., C. R. Ferguson, and E. F. Wood, 2013: Temporal variability of land–atmosphere coupling and its implications for drought over the southeast United States. *J. Hydrometeor.*, **14**, 622–635, https://doi.org/10.1175/JHM-D-12-090.1.

——, ——, and ——, 2014: Impact of land-atmospheric coupling in CFSv2 on drought prediction. *Climate Dyn.*, **43**, 421–434, https://doi.org/10.1007/s00382-013-1982-7.

Santanello, J. A., M. A. Friedl, and W. P. Kustas, 2005: An empirical investigation of convective planetary boundary layer evolution and its relationship with the land surface. *J. Appl. Meteor.*, **44**, 917–932, https://doi.org/10.1175/JAM2240.1.

——, J. Roundy, and P. A. Dirmeyer, 2015: Quantifying the land-atmosphere coupling behavior in modern reanalysis products over the U.S. Southern Great Plains. *J. Climate*, **28**, 5813–5829, https://doi.org/10.1175/JCLI-D-14-00680.1.

Segal, M., R. W. Arritt, C. Clark, R. Rabin, and J. Brown, 1995: Scaling evaluation of the effect of surface characteristics on potential for deep convection over uniform terrain. *Mon. Wea. Rev.*, **123**, 383–400, https://doi.org/10.1175/1520-0493(1995)123<0383:SEOTEO>2.0.CO;2.

Seneviratne, S. I., D. Lüthi, M. Litschi, and C. Schär, 2006: Land atmosphere coupling and climate change in Europe. *Nature*, **443**, 205–209, https://doi.org/10.1038/nature05095.

——, T. Corti, E. L. Davin, M. Hirschi, E. B. Jaeger, I. Lehner, B. Orlowsky, and A. J. Teuling, 2010: Investigating soil moisture climate interactions in a changing climate: A review. *Earth-Sci. Rev.*, **99**, 125–161, https://doi.org/10.1016/j.earscirev.2010.02.004.

Siqueira, M., G. Katul, and A. Porporato, 2009: Soil moisture feedbacks on convection triggers: The role of soil–plant hydrodynamics. *J. Hydrometeor.*, **10**, 96–112, https://doi.org/10.1175/2008JHM1027.1.

Song, H.-J., C. R. Ferguson, and J. K. Roundy, 2016: Land–atmosphere coupling at the Southern Great Plains Atmospheric Radiation Measurement (ARM) field site and its role in anomalous afternoon peak precipitation. *J. Hydrometeor.*, **17**, 541–556, https://doi.org/10.1175/JHM-D-15-0045.1.

Stull, R., 1988: *An Introduction to Boundary Layer Meteorology*. Springer, 670 pp.

Tawfik, A. B., and P. A. Dirmeyer, 2014: A process-based framework for quantifying the atmospheric preconditioning of surface-triggered convection. *Geophys. Res. Lett.*, **41**, 173–178, https://doi.org/10.1002/2013GL057984.

——, ——, and J. A. Santanello, 2015: The heated condensation framework. Part II: Climatological behavior of convective initiation and land–atmosphere coupling over the conterminous United States. *J. Hydrometeor.*, **16**, 1946–1961, https://doi.org/10.1175/JHM-D-14-0118.1.

Taylor, C. M., D. J. Parker, and P. P. Harris, 2007: An observational case study of mesoscale atmospheric circulations induced by soil moisture. *Geophys. Res. Lett.*, **34**, L15801, https://doi.org/10.1029/2007GL030572.

Tennekes, H., 1973: A model for the dynamics of the inversion above a convective boundary layer. *J. Atmos. Sci.*, **30**, 558–567, https://doi.org/10.1175/1520-0469(1973)030<0558:AMFTDO>2.0.CO;2.

Trenberth, K. E., 1999: Atmospheric moisture recycling: Role of advection and local evaporation. *J. Climate*, **12**, 1368–1381, https://doi.org/10.1175/1520-0442(1999)012<1368:AMRROA>2.0.CO;2.

Tuttle, J. D., and C. A. Davis, 2006: Corridors of warm season precipitation in the central United States. *Mon. Wea. Rev.*, **134**, 2297–2317, https://doi.org/10.1175/MWR3188.1.

van Heerwaarden, C. C., J. Vilà-Guerau de Arellano, A. F. Moene, and A. A. M. Holtslag, 2009: Interactions between dry-air entrainment, surface evaporation and convective boundary-layer development. *Quart. J. Roy. Meteor. Soc.*, **135**, 1277–1291, https://doi.org/10.1002/qj.431.

——, ——, A. Gounou, F. Guichard, and F. Couvreux, 2010: Understanding the daily cycle of evapotranspiration: A method to quantify the influence of forcings and feedbacks. *J. Hydrometeor.*, **11**, 1405–1422, https://doi.org/10.1175/2010JHM1272.1.

van Stratum, B. J. H., J. Vilà-Guerau de Arellano, C. C. van Heerwaarden, and H. G. Ouwersloot, 2014: Subcloud-layer feedbacks driven by the mass flux of shallow cumulus convection over land. *J. Atmos. Sci.*, **71**, 881–895, https://doi.org/10.1175/JAS-D-13-0192.1.

Vick, E. S., P. C. Stoy, A. C. Tang, and T. Gerken, 2016: The surface-atmosphere exchange of carbon dioxide, water, and sensible heat across a dryland wheat-fallow rotation. *Agric. Ecosyst. Environ.*, **232**, 129–140, https://doi.org/10.1016/j.agee.2016.07.018.

Wu, C.-M., B. Stevens, and A. Arakawa, 2009: What controls the transition from shallow to deep convection? *J. Atmos. Sci.*, **66**, 1793–1806, https://doi.org/10.1175/2008JAS2945.1.

Yamada, H., 2008: Numerical simulations of the role of land surface conditions in the evolution and structure of summertime thunderstorms over a flat highland. *Mon. Wea. Rev.*, **136**, 173–188, https://doi.org/10.1175/2007MWR2053.1.

Yin, J., J. D. Albertson, J. R. Rigby, and A. Porporato, 2015: Land and atmospheric controls on initiation and intensity of moist convection: CAPE dynamics and LCL crossings. *Water Resour. Res.*, **51**, 8476–8493, https://doi.org/10.1002/2015WR017286.